Journal of Nanofluids
Vol. 11, pp. 74–83, 2022
(www.aspbs.com/jon)

ARTICLE

Magnetohydrodynamics Boundary Layer Flow of Hybrid Nanofluid in a Thin-Film Over an Unsteady Stretching Permeable Sheet

Nur Ilyana Kamis, Lim Yeou Jiann, Sharidan Shafie, Taufiq Khairi Ahmad Khairuddin, and Md Faisal Md Basir*

Department of Mathematical Sciences, Faculty of Science, Universiti Teknologi Malaysia, 81310 UTM Johor Bahru, Johor, Malaysia

This analysis explored the computational process of heat transfer analysis in a thin-film MHD flow embedded in the hybrid nanoparticles, which combine the spherical copper and alumina dispersed in ethylene glycol as the conventional heat transfer Newtonian fluid model over a stretching sheet. The nonlinear ordinary differential equations (ODEs) was attained by transforming partial differential equation (PDEs) as governing equations when implementing the similarity transformations technique. The resulting nonlinear ODEs have been utilized by using the Keller box method. The natures of the thin-film flow and heat transfer through the various values of the pertinent parameters: unsteadiness, nanoparticle volume fraction, thin-film thickness, magnetic interaction and intensity suction/injection are deliberated. The approximate results for velocity and temperature distributions and physical quantities in terms of local skin friction and Nusselt number have been obtained and analyzed via graphs and tables. As a consequence, the suction expresses a more prodigious effect on the hybrid nanofluid rather than injection fluid for all the investigation parameters. It is worth acknowledging that the existence of the nanoparticles and MHD in the viscous hybrid nanofluid tends to enhance the temperature profile but decay the particle movement in the thin-film flow. It is perceived that the velocity and temperature profiles decline for the growth of the unsteadiness, thin-film thickness and suction/injection parameters.

KEYWORDS: Thin-Film Flow, Hybrid Nanofluid, Suction/Injection, MHD, Keller Box Method.

1. INTRODUCTION

Thin-film flow is the essential part of the microfabrication industry where it constructs the physical objects with dimensions in the micrometer to millimeter range. The products that use multiple thin-film flow include electronic devices containing conductive metals that allow the electricity flow and medical devices that used chemical films to inhibit microbial growth. Therefore, these activities encouraged the researchers to study and analyze the several effects on heat transfer in a thin film flow across moving vertical, horizontal and slanted flat plates. Moreover, the principle utilization of such thin-film fluid is in draining, coating, wetting, biological and solar cells as given in Bertozzi,[1] Roy et al.,[2] Dutta et al.,[3] Taherzadeh,[4] Liu et al.,[5] Kreder et al.,[6] Girtan,[7] Girtan[8] and Thiele.[9] It is produced through a process called 'Thin-Film Decomposition,' which is a process of applying the thin-film onto a surface that is to be coated.[10]

The first problem of this phenomenon has been explored by Wang[11] without considering the heat transfer. Wang[11] studied the issue of thin-film flow in the Newtonian fluid that has been motivated by the studies of Sakiadis,[12] Crane,[13] Carragher and Crane[14] who studied the theoretical technique to solve the heat transfer flow along with the stretching sheet. The study found that the rare exact similarity solution of the unsteady Navier-Stokes equation and an investigation on integration for that equation is needed. Therefore, Andersson et al.[15] started an analysis to explore the nature of the hydrodynamic heat transfer problem solved by Wang.[11] Andersson et al.[15] extended the work done by Wang[11] and introduced the similarity transformation for the thermal equation. The author found that the temperature on the thin-film flow enlarges from the elastic sheet towards the free surface. After that, Wang[16] explored the flow problem with heat transfer. The HAM method was applied to attain the investigated parameters unsteadiness and Prandtl number towards velocity and temperature profiles. As a result, different values of

*Author to whom correspondence should be addressed.
Email: mfaisalmbasir@utm.my
Received: 19 August 2021
Accepted: 9 September 2021

parameters tend to vary in the thickness of the thin-film. Shear stress between the wall of thin-film and fluid flow was enlarged but decreased in thin-film thickness due to increasing the unsteadiness parameter that pointed out the stretching rate of the plane. The heat transfer of the thin-film flow has been declined by the enhancement of the Prandtl number.

The development in science and technology is levitating the demand for characterized devices with the best performances and optimum functioning. Therefore, the researcher introduced a new class of fluids using nanoparticles named nanofluid.[17] The existence of the nanoparticles in the fluid can improve the rate of change of the heat and working fluid properties due to their special properties.[18] According to Choi[17] who proposed the metallic or non-metallic particles that have a high thermal conductivity in a fluid can tends to uplift the superior of heat transfer. The incorporates of nanoparticles and fluid can reduce the boiling performance and degradation increased. Most importantly, it smoother the surface of nucleate sites, hence considerable deterioration of the heat transfer coefficient.[19, 20] The scholar and scientists have reported the dissolving of the nanoparticles in the conventional fluid included Khan and Pop,[21] Yirga and Shankar,[22] Pourmehran et al.,[23] Jahan et al.,[24] Hafidz et al.[25] and Gangadhar et al.[26] Yirga and Shankar[22] studied the MHD flow and heat transfer analysis in a steady porous sheet under the effect of viscous dissipation and chemical reaction. The transformed governing equations were solved numerically by implementing the Keller box method.

The presence of the nanoparticle volume fraction in the porous sheet has increased the skin friction. Moreover, Jahan et al.[24] discussed an unsteady and heat transfer analysis under the effect of suction/injection in a nanofluid. Consequently, suction/injection parameters in the nanofluid have a huge impact on the physical quantities as well as velocity and temperature fields. The nanofluids MHD together with the suction/injection effects for the several geometries have been cross-examined by Krishna and Chamkha,[27] Krishna and Chamkha[28] as well as Chamkha et al.[29] The studies claimed that the suction effect boosts the heat transfer rate of the nanofluid. Hazarika et al.[30] studied the thermophoresis and viscous dissipation of MHD nanofluid over a porous stretching sheet. The author considered the copper, Argentum and ferum (III) oxide as the nanoparticles. Control-volume-based finite element method (CVFEM) as the numerical method has been employed by Chamkha et al.[31] to analyze the trend of nanoparticles in natural convection flow. A similar method was also applied by Dogonchi et al.[32] when solving the mathematical modeling of magnetic nanofluid natural convection in the porous with Brownian motion. In addition, Dogonchi et al.[33] claimed that the increase of the suction parameter leads to an increase in the velocity, however, a decline in the temperature of the nanofluid.

Based on the previous publications, nanofluids performed well and showed a positive effect on heat transfer. This situation encouraged the researcher to think about incorporating of the different nanoparticles and known as hybrid nanofluids. Several researchers have cross-examined the combinations of alumina and copper since these combinations have enhanced the thermal conductivity and increased the convective heat transfer. For example, Devi and Devi[34] studied the effect of suction parameters on MHD copper/alumina dissolved in water as a conventional fluid. This analysis showed the upsurge of the suction intensity retards the velocity and temperature profiles as well as skin friction coefficient, however it overshot the Nusselt number representing the nanofluid's heat transfer rate. Devi and Devi[35] extended the research done by Devi and Devi[34] by considering the Lorentz force and Newtonian heating in a three-dimensional hybrid nanofluid model. Momentum boundary layer thickness turned thinner as increasing the Lorentz force through the enhanced value of the magnetic interaction parameter M. The Lorentz force heated the particles of hybrid nanofluid, $Cu–Al_2O_3$ thereby, the thermal boundary layer gets thicker.

Besides, Devi and Devi[36] compared the numerical model for thermal conductivity of $Cu–Al_2O_3$ with the experimental data from Suresh et al.[37] when using the 90:10 ratio concentration of $Cu–Al_2O_3$/water. During this analysis, the various volume fraction nanoparticles such as 0.1%, 0.33%, 0.75%, 1% and 2% give an excellent agreement with the experimental data. Quite interesting results, the growth of nanoparticles volume fraction from 0.005 to 0.06 has enhanced the temperature profile, thereby overshoot the fluid's heat transfer rate. Nevertheless, the velocity profile, as well as the wall shear stress, were retarded. It is worth mentioning that the works from[34–36] depict that the heat transfer rate of hybrid nanofluid is higher than nanofluid. Series works from[34–36] have motivated Waini et al.[38–40] to investigate similar combination nanoparticles with different effects past a stretching/shrinking sheet. In the research, the stability analysis was performed to determine the dual solutions in the long run and it is claimed that the upper branch solution is stable. Further, Ghalambaz et al.[41] reported that the presence of the hybrid nanoparticles has a positive effect on the heat transfer rate of the hybrid nanofluid. Tayebi and Chamkha[42] conducted a numerical analysis of steady MHD natural convective heat transfer and flow on hybrid nanofluid, alumina and copper which dissolved in water as a Newtonian fluid model.

Moreover, several effects such as the existence of the magnetohydrodynamics (MHD) and suction/injection in fluid grabbed the response of industry especially engineering to explore deeply the flow of the fluid as well as the production of the products past in different geometries. VeeraKrishna et al.[43] studied the analysis of second-grade fluid with MHD together with the hall effects through

ARTICLE

the porous medium between two vertical plates. Besides, porous medium with ramped wall temperature and surface concentration in MHD second grade fluid have been done by VeeraKrishna and Chamkha.[44] The characteristics of heat and mass transfer on MHD flow of second-grade fluid together with the porous medium subjected to a semi-infinite vertical stretching sheet also have been investigated by Krishna et al.[45] The fluid under the impacts of MHD in porous plate also gives the significant changes of the fluid in free convection flow.[46,47] Further, Veera Krishna et al.[48] explored the MHD, ion slip and porous parameter on unsteady generating/absorbing second-grade fluid.

Clearly from the above literature review, the study on heat transfer in a thin-film with hybrid nanoparticles (alumina-copper) has not yet been discussed anywhere by any researchers. Therefore, the present problem follows closely the work done by[16,34–36] by including the hybrid nanofluid. The Keller box method is to be utilized to obtain the numerical solutions. The details of the method can be found in the book by Cebeci and Bradshaw.[49] In dealing with the nonlinear parabolic problem, this method is quite appropriate and widely used by many researchers like,[22,50] and Ref. [51] to solve problems of similar nature (nonlinear parabolic problems) which has been proven to be efficient. The implicit Keller box method is an unconditionally stable finite difference method conjunction with achieves remarkable accuracy. The effects of several parameters on the flow and heat transfer analysis are presented in form of the graphs and tables. The resultant numerical results will be compared with the published paper to show reliability in the numerical method employed.

2. MATHEMATICAL FORMULATION

An unsteady two-dimensional, incompressible, laminar boundary layer flow of an electrically conducting and MHD thin-film flow of hybrid nanofluid across the porous stretching sheet has been considered. The fluid flow in the thin-film with uniform thin-film thickness $h(t)$ is caused by the stretching sheet at x-axis with velocity U_w and y is normal to the sheet. The sheet is assumed to have a mass transfer parameter with a velocity of the suction/injection, V_w while the temperature of the sheet, T_w varies with the distance x along with the sheet. The stretched velocity, mass transfer parameter, and temperature at the sheet are in the form of $U_w = bx/(1-\alpha t)$, $V_w = (V_w)_0/(1-\alpha t)^{1/2}$ and $T_w = T_0 - T_{\text{ref}}(bx^2/(2\nu))(1-\alpha t)^{-3/2}$ respectively. Here, $(V_w)_0$ it corresponds to the initial velocity suction/injection parameter. The viscous hybrid nanofluid is being sucked with velocity and injected at the thin film's sheet. T_0 represents for the variable of slit temperature and reference temperature T_{ref}. Further, $\alpha > 0$ and $b > 0$ are taken for the following analyses and are valid only for a time $t < \alpha^{-1}$. The geometry of the problem is portrayed in Figure 1.

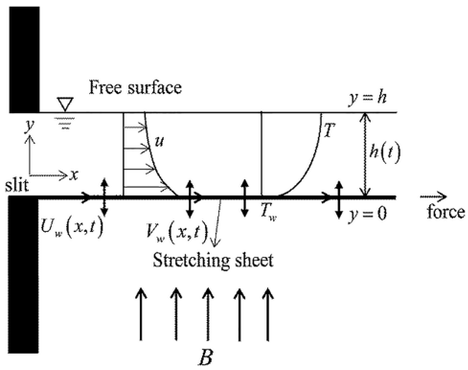

Fig. 1. Physical model.

The governing PDEs for MHD viscous hybrid nanofluid with the extent of the Tiwari and Das[52] model for hybrid nanofluid can be written as[53]

$$\frac{\partial u}{\partial x} + \frac{\partial v}{\partial y} = 0, \tag{1}$$

$$\rho_{hnf}\left[\frac{\partial u}{\partial t} + u\frac{\partial u}{\partial x} + v\frac{\partial u}{\partial y}\right] = \mu_{hnf}\frac{\partial^2 u}{\partial y^2} + \sigma_{hnf}B^2(t)u, \tag{2}$$

$$(\rho c_p)_{hnf}\left(\frac{\partial T}{\partial t} + u\frac{\partial T}{\partial x} + v\frac{\partial T}{\partial y}\right) = k_{hnf}\frac{\partial^2 T}{\partial y^2}, \tag{3}$$

where velocity segments along x and y direction is (u, v). k_{hnf} represents the conduction by the heat of nanodispersion, the density for the hybrid nanofluids ρ_{hnf}, $(C_\rho)_{hnf}$ indicates the energy capacity of nanodispersion, μ_{hnf} demonstrating an effective dynamic viscosity and σ_{hnf} corresponds to the electrical conductivity for the hybrid nanofluid. T and t are demonstrate the temperature and time. A uniform magnetic $B(t)$ which is dependent on time, is applied perpendicular to the sheet. The magnetic Reynolds number is assumed to be small to neglect the induced magnetic field. The effect of the Lorentz force is negligible. The polarization of charges on an electric field is taken to be zero. The $B(t)$ for the flow under this investigation can be defined in the form of the variable of Ref. [53]

$$B(t) = B_0(1-\alpha t)^{-(1/2)} \tag{4}$$

The boundary conditions that are associated with these equations are Ref. [16]

$$y = 0: u = U_w, \quad v = V_w, \quad T = T_w, \tag{5}$$

$$y = h: \frac{\partial u}{\partial y} = \frac{\partial T}{\partial y} = 0, \quad v = \frac{dh}{dt}, \tag{6}$$

The spherical hybrid nanoparticles, alumina, and copper are taken as dispersing nanoparticles. Ethylene glycol fluid is considered the Newtonian base fluid. The thermophysical properties of the nanoparticles and base fluid with the addition of electrical conductivity can be written as in Table I.

Table I. Thermophysical properties of the base fluid and nanoparticles.[34, 54]

Physical properties	Water plus 30% ethylene glycol	Cu	Al_2O_3
C_p ($Jkg^{-1}K^{-1}$)	3714	385	765
ρ (kgm^{-3})	1038	8933	3970
k ($Wm^{-1}K^{-1}$)	0.484	400	400
σ (s/m)	0.00276	5.96×10^6	35×10^6
Pr	16.62	-	-

The governing Eqs. (1)–(3) along together with the boundary conditions (5) and (6) are reduced into the simplest set of ODEs by using the similarity transformations technique. Wang[16] introduced the following dimensionless variable in vector $f(\eta)$ and $\theta(\eta)$, and are presented as

$$\psi = [\nu b(1-\alpha t)^{-1}]^{1/2} x\xi f(\eta), \tag{7}$$

$$T = T_0 - T_{ref}\left(\frac{bx^2}{2\nu}\right)(1-\alpha t)^{-(3/2)}\theta(\eta), \tag{8}$$

$$\eta = \left(\frac{\nu}{b}\right)(1-\alpha t)^{-(1/2)}\xi^{-1} y, \tag{9}$$

where ξ is an undefined constant which denotes the film's dimensionless thickness. At the free surface, $\eta = 1$ and $y = h(t)$, Eq. (8) has been rewritten as

$$\begin{aligned}\xi &= \left(\frac{\nu}{b}\right)(1-\alpha t)^{-(1/2)} y \\ &= \left(\frac{\nu}{b}\right)(1-\alpha t)^{-(1/2)} h(t),\end{aligned} \tag{10}$$

which gives

$$\begin{aligned} h(t) &= \xi\left(\frac{\nu}{b}\right)(1-\alpha t)^{1/2} h(t) \\ \frac{dh}{dt} &= \tfrac{1}{2}\xi\left(\tfrac{\nu}{b}\right)(1-\alpha t)^{-(1/2)}(-\alpha) \\ &= -\frac{1}{2}\alpha\xi\left(\frac{\nu}{b}\right)(1-\alpha t)^{-(1/2)}, \end{aligned} \tag{11}$$

and stream function, $\psi(x, y, t)$ which can be defined as

$$u = \frac{\partial\psi}{\partial y} \quad \text{and} \quad v = -\frac{\partial\psi}{\partial x} \tag{12}$$

By using the Eqs. (6) and (11), we have.

$$u = \frac{bx}{(1-\alpha t)} f', v = -\left(\frac{\nu b}{1-\alpha t}\right)^{1/2}\xi f. \tag{13}$$

Equation (13) automatically satisfies the continuity Eq. (1). Now, by imposing the Eqs. (7)–(9) and (13) coupled with the physical properties of hybrid nanofluids into Eqs. (2)–(3) and (5)–(6), and we have.

$$\begin{aligned}\left(\frac{A_1}{A_2}\right) f''' + \lambda\Bigg[ff'' - f'^2 - S\left(f' + \frac{1}{2}\eta f''\right) \\ - \left(\frac{A_3}{A_4}\right) M f'\Bigg] = 0,\end{aligned} \tag{14}$$

$$\left(\frac{A_5}{A_6}\right) Pr^{-1}\theta'' + \lambda\left[-S\left(\frac{3}{2}\theta + \frac{1}{2}\eta\theta'\right) - 2f'\theta + f\theta'\right] = 0. \tag{15}$$

and the boundary conditions (5) and (6) becomes.

$$\eta = 0: f'(0) = 1, \quad f(0) = w, \quad \theta(0) = 1, \tag{16}$$

$$\eta = 1: f''(1) = 0, \quad \theta'(1) = 0, \quad f(1) = \frac{S}{2}. \tag{17}$$

where a prime denotes the differentiation concerning η. The parameter $A(i = 1, \ldots, 6)$ is the modification of the thermophysical properties for the hybrid nanofluids that can be defined as

$$\begin{aligned} A_1 &= \frac{1}{[1-(\phi_1+\phi_2)]^{2.5}}, \\ A_2 &= \left[(1-\phi_2)\phi_1\frac{\rho_{s_1}}{\rho_{bf}} + \phi_2\frac{\rho_{s_2}}{\rho_{bf}} + (1-\phi+\phi_1\phi_2)\right], \\ A_3 &= \left[\frac{\sigma_{s_2} + 2\sigma_{nf} - 2\phi_2(\sigma_{nf} - \sigma_{s_2})}{\sigma_{s_2} + 2\sigma_{nf} + \phi_2(\sigma_{nf} - \sigma_{s_2})}\right] \\ &\quad \times \left[\frac{\sigma_{s_1} + 2\sigma_{bf} - 2\phi_1(\sigma_{bf} - \sigma_{s_1})}{\sigma_{s_1} + 2\sigma_{bf} + \phi_1(\sigma_{bf} - \sigma_{s_1})}\right], \end{aligned}$$

where

$$\begin{aligned} \sigma_{nf} &= \left[\frac{\sigma_{s_1} + 2\sigma_{bf} - 2\phi_1(\sigma_{bf} - \sigma_{s_1})}{\sigma_{s_1} + 2\sigma_{bf} + \phi_1(\sigma_{bf} - \sigma_{s_1})}\right]\sigma_{bf}, \\ A_4 &= \frac{(1-\phi_2)[(1-\phi_1)\rho_{bf} + \phi_1\rho_{s_1}] + \phi_2\rho_{s_2}}{\rho_{bf}}, \\ A_5 &= \left[\frac{k_{s_2} + 2k_{nf} - 2\phi_2(k_{bf} - k_{s_2})}{k_{s_2} + 2k_{nf} + \phi_2(k_{bf} - k_{s_2})}\right] \\ &\quad \times \left[\frac{k_{s_1} + 2k_{bf} - 2\phi_1(k_{bf} - k_{s_1})}{k_{s_1} + 2k_{bf} + \phi_1(k_{bf} - k_{s_1})}\right] \end{aligned} \tag{18}$$

where

$$\begin{aligned} k_{nf} &= \left[\frac{k_{s1} + 2k_{bf} - 2\phi_1(k_{bf} - k_{s_1})}{k_{s_1} + 2k_{bf} + \phi_1(k_{bf} - k_{s_1})}\right]k_{bf}, \\ A_6 &= \left[(1-\phi_2)\phi_1\frac{(\rho c_p)_{s_1}}{(\rho c_p)_{bf}} + \phi_2\frac{(\rho c_p)_{s_2}}{(\rho c_p)_{bf}} + (1-\phi+\phi_1\phi_2)\right], \end{aligned}$$

Here, λ is the thin film thickness, unsteadiness of the dimensionless measure is denoted by S, Pr is the Prandtl number, suction/injection parameter is presented by w and the magnetic interaction parameter, M and are defined as.

$$\begin{aligned} \lambda = \xi^2, \quad S = \frac{\alpha}{b}, \quad Pr = \frac{(\mu c_p)_{bf}}{k_{bf}}, \\ w = -\frac{(V_w)_0}{\xi\sqrt{\nu b}}, \quad M = \frac{\sigma_{bf} B_0^2}{\rho_{bf} b} \end{aligned} \tag{19}$$

The physical quantities that are concerned in the present study are the local skin fraction, C_f which depicts the wall shear stress, $\tau_w(x)$ and the heat transfer rate $q_w(x)$ that is shown through the Nusselt number, Nu_x, which are written as

$$C_f = \frac{\tau_w(x)}{\rho_f u_w^2} \quad \text{and} \quad Nu_x = \frac{xq_w(x)}{k_f(T_w - T_\infty)}. \tag{20}$$

$\tau_w(x)$ and $q_w(x)$ are defined as,[24]

$$\tau_w(x) = \mu_{hnf}\left(\frac{\partial u}{\partial y}\right)_{y=0}, \tag{21}$$

$$q_w(x) = -k_w\left(\frac{\partial T}{\partial y}\right)_{y=0}. \tag{22}$$

Using similarity variables (6)–(8), the dimensionless local skin friction and heat transfer coefficient can be represented as.

$$C_f \mathrm{Re}^{1/2} = \frac{1}{\delta}\left[\frac{1}{(1-\phi_1)^{2.5}+(1-\phi_2)^{2.5}}\right] f''(0), \tag{23}$$

$$Nu_x \mathrm{Re}^{-1/2} = -\frac{1}{\delta}\left(\frac{k_{hnf}}{k_f}\right)\theta'(0). \tag{24}$$

where Reynold number, $\mathrm{Re} = xu_w/\nu_f$.

3. NUMERICAL APPROACH

The transformed nonlinear coupled Eqs. (14) and (15) along with the corresponding boundary conditions (16) and (17) in the form of ODEs are solved numerically using an unconditionally stable implicit finite difference method known as the Keller box method. The numerical solution is attained by following a couple of steps as below.

(i) Reduce higher order of ordinary differential Eqs. (14) and (15) into the system of first-order ordinary differential equations by introducing the new dependent variables $f = f$, $f' = u$, $f'' = v$, $\theta = \theta$, $\theta' = g$. Hence, yield

$$\left(\frac{A_1}{A_2}\right)v' + \lambda\left[fv - \frac{1}{2}S\eta v - u^2 - Su - \left(\frac{A_3}{A_4}\right)Mu\right] = 0, \tag{25}$$

$$\left(\frac{A_5}{A_6}\right)Pr^{-1}g' + \lambda\left(fg - 2\theta u - \frac{1}{2}S\eta g - \frac{3}{2}S\theta\right) = 0. \tag{26}$$

and the boundary conditions (14) and (15) becomes;

$$\eta = 0: f = 0, \quad u = 1, \quad \theta = 1, \tag{27}$$

$$\eta = 1: f = \frac{S}{2}, \quad v = 0, \quad g = 0. \tag{28}$$

(ii) Implementing the central difference scheme to write the finite differences for the transformed first-order ODEs. Generally, the derivatives in the η-direction are defined as (see Fig. 2)

$$p' = \frac{\partial p}{\partial \eta} = \frac{p_j - p_{j-1}}{h_j}$$

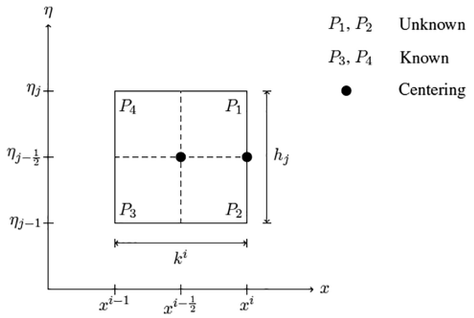

Fig. 2. Net rectangle for difference approximation.

and for any points generally, we have.

$$p_{j-\frac{1}{2}} = \frac{1}{2}(p_j - p_{j-1})$$

(iii) Linearize the nonlinear algebraic system by using the Newton method. Introducing the iterates for the new independent variables. For example;

$$f_j^{(i+1)} = f_j^{(i)} + \delta f_j^{(i)}$$

(iv) Solve the linear system in matrix form by the block elimination technique. The matrix is written in the form of

$$[A][\delta] = [r], \tag{29}$$

where matrix A is zero, excluding those three along the diagonal. Then, the vector-matrix can be written as

$$\begin{bmatrix} [A_1] & [C_1] & & & & & \\ [B_2] & [A_2] & [C_2] & & & & \\ & \ddots & \ddots & & & & \\ & & \ddots & & & & \\ & & & [B_{j-2}] & [A_{j-2}] & [C_{j-2}] & \\ & & & & [B_J] & [A_J] & \end{bmatrix} \times \begin{bmatrix} [\delta_1] \\ [\delta_2] \\ \vdots \\ \vdots \\ \vdots \\ [\delta_{j-1}] \\ [\delta_J] \end{bmatrix} = \begin{bmatrix} [r_1] \\ [r_2] \\ \vdots \\ \vdots \\ \vdots \\ [r_{j-1}] \\ [r_J] \end{bmatrix}, \tag{30}$$

4. RESULTS AND DISCUSSION

4.1. Validation of the Results

Approval of the method and the computational code is done by looking at the mathematical consequences of the

current examination with Wang[16] and Das et al.[20] Table II provides a comparison of the numerical findings with previous publications by setting the parameters; nanoparticles volume fraction $\phi_1 = \phi_2 = 0$, suction/injection $w = 0$, Prandtl number $Pr = 1.0$, magnetic $M = 0$ for several thin-film thicknesses λ which are subjected to a different parameter S. The value of the local skin friction $f''(0)$ as depicted in the table shows an excellent agreement with the previous work. Hence, the code authentication is reasonable. By increasing the unsteadiness parameter S, it $f''(0)$ also increases.

4.2. Numerical Results

The hybrid nanofluid flow and heat transfer behaviour in a thin-film is separated into two cases; suction $(w > 0)$ and injection $(w > 0)$ fluid through a permeable porous sheet when the sheet is stretching. The numerical solutions are obtained for various physical parameters values to explain in-depth the physical problems in the form of the flow structure relating to velocity, temperature, local skin friction, and reduced Nusselt number coefficient.

Figure 3 indicates that the velocity profile decays as the parameter of M is improved for all cases ($w < 0$ or $w > 0$). The enhancement of the retarding force upsurge in the hybrid nanofluid is associated with the increase of M, which lessens the motion of the hybrid nanoparticles and results in a thinning momentum boundary layer thickness. The temperature profile in Figure 4 drawn the opposite pattern as parameter M rises. A similar nature for both profiles was observed and reported by Devi and Devi[34] and Upreti et al.[55] This is because the electromagnetic in the fluid escalates as M intensifies, thereby implying the strong Lorentz's force, which generates friction in the hybrid nanofluid. It is detected from the figure, and the thermal boundary layer changes to thicken with the build-up of friction under the impact of the magnetic field. Moreover, the minimum velocity profile and the maximum temperature profile for the magnetic hybrid nanofluid are archived by the injection than the suction effects. A similar trend of temperature profile for suction and injection fluids flow was reported by Pal.[56]

The impact of the unsteadiness parameter S on the velocity and temperature distributions are depicted, respectively, in Figures 5 and 6 for both suction and injection

Table II. Comparison of $f''(0)$ for $\phi_1 = \phi_2 = w = M = 0$, $Pr = 1.0$ and several values of λ as S varies.

	$f''(0)$		
S	Das, Acharya and Kundu[20]	Wang[16]	Present
0.8	−2.6809	−2.6809	−2.6805
1.0	−1.9724	−1.9724	−1.9721
1.2	−1.4444	−1.4426	−1.4425
1.4	−1.0128	−1.0128	−1.0127
1.6	−0.6424	−0.6424	−0.6441

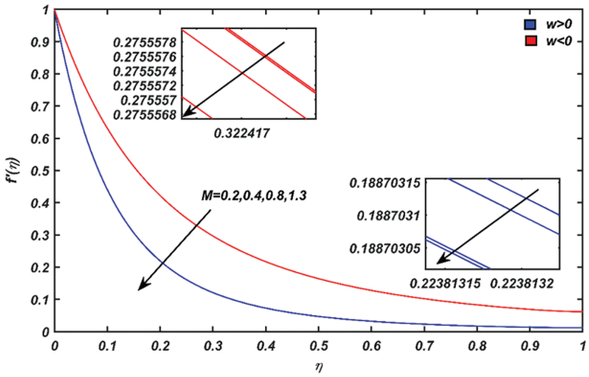

Fig. 3. Velocity distribution for various values of M.

cases. It can be concluded that an enhances in S declines the velocity and temperature profiles. Physically, the rate of the initial sheet to stretch from the narrow-slit failures due to the growth of the unsteadiness parameter thereby decline the force to flow the fluid in the thin-film. This situation retards the velocity of the molecules' movement and inhibits the particles to absorb the heat. The momentum and thermal boundary layer thickness also reduced when S increased. As expected, the velocity and temperature profiles of the hybrid nanofluid under the effect of suction are lower than the injection case. It is perceived that a larger amplitude of S leads to more thinning of both boundary layer thickness in the suction case compared to the injection case.

Figure 7 elucidates the nanoparticles volume fraction's variation towards the velocity profile of the magnetic hybrid nanofluid. It is noticeable that the velocity profile of the hybrid nanoparticles drops off when the volume fraction of the copper nanoparticles increases from 0.005 to 0.06. Further, the momentum boundary layer thickness is diminished and therefore slows down the fluid motion. This is because of the boost up of the viscosity in the fluid when the fluid is concentrated with the nanoparticles. The movement of the particles in the thin-film under the effect of the intensity of injection is faster than in the

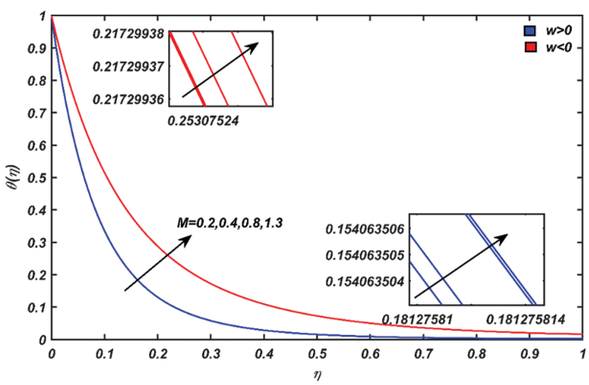

Fig. 4. Temperature distribution for various values of M.

ARTICLE

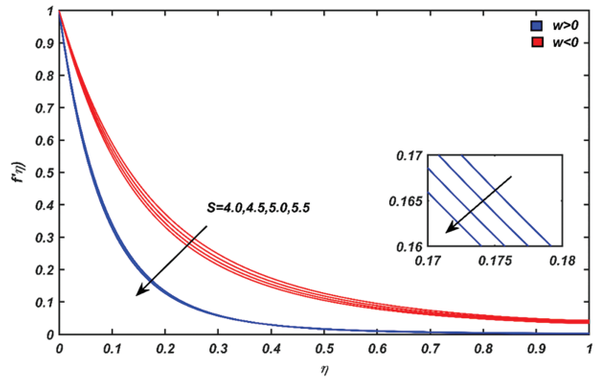

Fig. 5. Velocity distribution for various values of S.

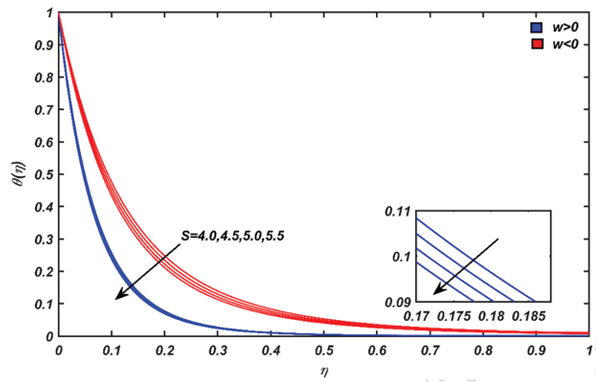

Fig. 6. Temperature distribution for various values of S.

situation of suction. The relation of the ϕ_2 and affected temperature profile is mapped in Figure 8. As proved by several researchers in the literature, the increasing of the ϕ_2 parameter results in an elevates the thermal conductivity of the fluid.

Consequently, the temperature of the magnetic hybrid nanofluid intensifies and leads to an enhancement in the thermal boundary layer thickness of the thin-film flow. Furthermore, it is worth mentioning that the injection case's temperature and thermal boundary layer thickness

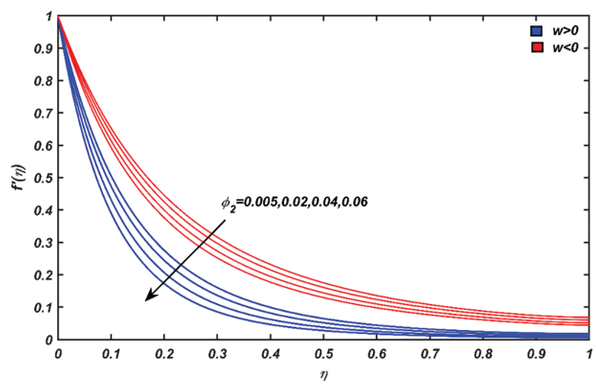

Fig. 7. Velocity distribution for various values of ϕ_2.

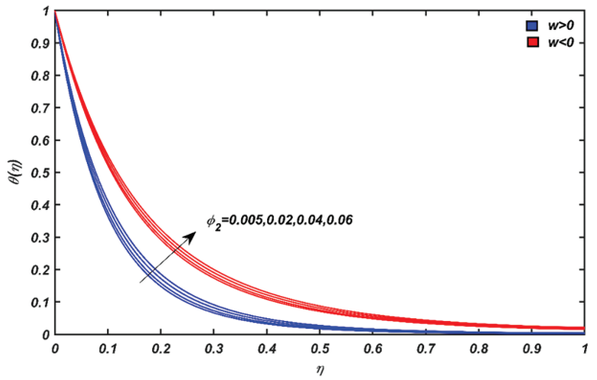

Fig. 8. Temperature distribution for various values of ϕ_2.

is greater than the suction case. Results from this research on velocity and temperature distributions concurred well with the theoretical outcome of Das et al.[57] for suction and injection of MHD nanofluid.

The variation tendency on the hybrid nanofluid velocity due to the thin-film thickness λ is demonstrated in Figure 9. Enhancement of the dimensionless parameter λ spells out the thicker of the thin-film thickness. The momentum boundary layer turns thinner since the particle of the molecules in the hybrid nanoparticles moves slowly, corresponding to the decrementation in the fluid velocity profile. In an injection fluid, the particle's velocity is higher than the suction fluid, and the same goes for the thickness of the momentum boundary layer. The thin-film thickness reduces the temperature profile of the magnetic hybrid nanofluid, as sketched in Figure 10. It is obvious because thicker thin-film thickness allows less heat absorption to the ambient fluid from the surface sheet, thus declines the thermal boundary layer thickness. From Figure 10, the magnetic hybrid nanofluid in the suction case has a lower temperature than in injection case.

The response of the velocity and temperature profiles due to the mass transfer parameter, the suction/injection parameter, is presented in Figures 11 and 12. The addition of the hybrid nanofluid particles to the thin-film by

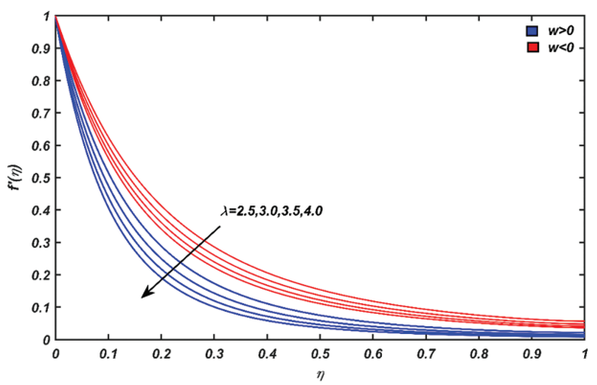

Fig. 9. Velocity distribution for various values of λ.

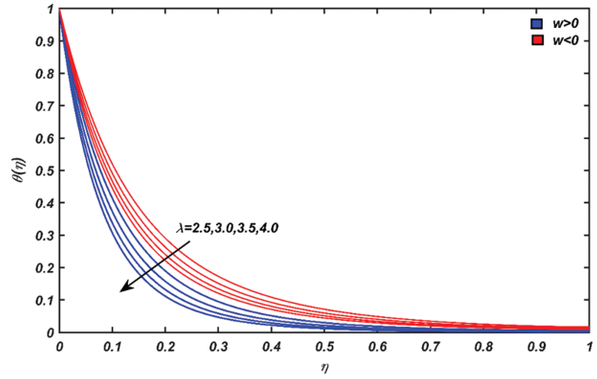

Fig. 10. Temperature distribution for various values of λ.

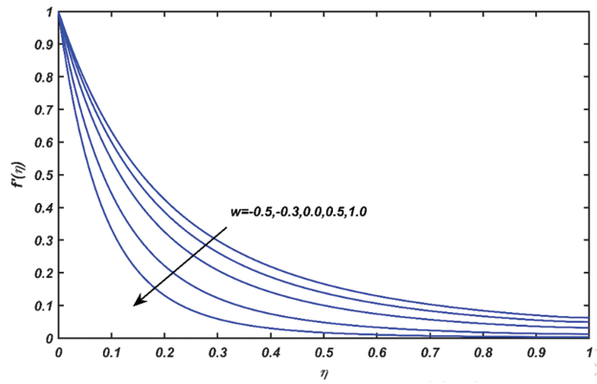

Fig. 11. Velocity distribution for various values of w.

implementing the injection's intensity shrinks the velocity and temperature profiles. Moreover, similar performances are obtained when the disposal of the hybrid nanofluid particles from the thin film under the suction effects through the permeable stretching sheet. The figures reveal that in both cases of the fluid, the momentum and thermal boundary layer thickness dwindle as increasing the parameter w. The suction of the fluid causes a speed reduction, and heat content in the particles is greater than under the injection fluid, as depicted in Figures 11 and 12.

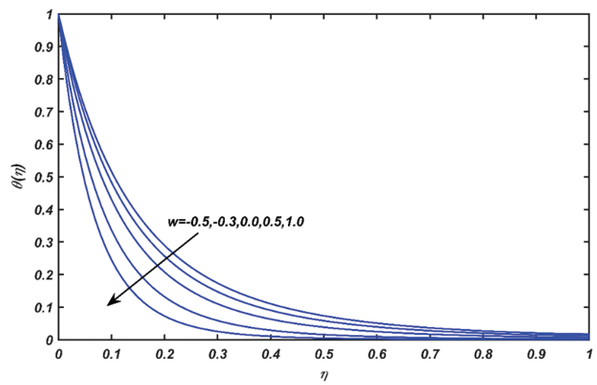

Fig. 12. Temperature distribution for various values of w.

Table III. Local skin friction $C_f\mathrm{Re}_x^{1/2}$ and Nusselt number, $Nu_x\mathrm{Re}_x^{-1/2}$ for suction and injection cases on the various values of M, S, ϕ_2 and λ.

				$C_f\mathrm{Re}_x^{1/2}$		$Nu_x\mathrm{Re}_x^{-1/2}$	
M	S	ϕ_2	λ	Suction, $w>0$	Injection, $w<0$	Suction, $w>0$	Injection, $w<0$
0.2				−12.3596	−6.7288	15.0216	8.5816
0.4				−13.3780	−7.78789	14.9917	8.5395
0.8				−14.2839	−8.7315	14.9668	8.5045
1.3				−15.1091	−9.5900	14.9454	8.4745
	4.0			−11.9977	−6.2363	14.4155	7.8467
	4.5			−12.1798	−6.4870	14.7229	8.2223
	5.0			−12.3596	−6.7288	15.0216	8.5816
	5.5			−12.5371	−6.9624	15.3123	8.9265
		0.005		−7.5230	−4.8292	10.5845	6.8098
		0.02		−9.3420	−5.1274	10.2235	6.6471
		0.04		−9.2614	−5.5278	9.7689	6.4388
		0.06		−10.3656	−5.9337	9.3420	6.2395
			1	−7.3615	−5.2865	9.3036	6.8887
			1.5	−8.2944	−5.7714	10.4545	7.5228
			2	−9.1933	−6.2144	11.5588	8.1024
			2.5	−10.0661	−6.6242	12.6273	8.6388

The influences of the various values of the governing parameter M, S, ϕ_2 and λ on local skin friction $C_f\mathrm{Re}_x^{1/2}$ and Nusselt number $Nu_x\mathrm{Re}_x^{-1/2}$ are mapped in Table III. An increment in the values dimensionless magnetic field parameter M unveils a slumping effect on $C_f\mathrm{Re}_x^{1/2}$ an equivalent behaviour in $Nu_x\mathrm{Re}_x^{-1/2}$. Sandeep et al.[53] also noticed this kind of characteristic, who considered an unsteady MHD nanofluid flow embedded with nanoparticles in a thin-film. The increase of the unsteadiness parameter S and thin-film thickness λ curtail the local skin friction, thereby decrease the magnitude of the wall shear stress. However, the heat transfer rate or the Nusselt number showed greater rates for higher parameter S and λ respectively. Thus, due to the Nusselt number's escalation, the fluid's convective heat transfer constantly increased.

Furthermore, the wall shear stress and the heat transfer rate slightly decline with the growth of nanoparticles volume fraction ϕ_2 for the magnetic hybrid nanofluid. Similar to the impact of the parameter w as tabulated in Table IV, the values of the $C_f\mathrm{Re}_x^{1/2}$ is decreased when the volume fraction is improved, but an opposite tendency is observed for the $Nu_x\mathrm{Re}_x^{-1/2}$.

Table IV. Local skin friction $C_f\mathrm{Re}_x^{1/2}$ and Nusselt number, $Nu_x\mathrm{Re}_x^{-1/2}$ on the various values of w.

Mass transfer parameter, w	$C_f\mathrm{Re}_x^{1/2}$	$Nu_x\mathrm{Re}_x^{-1/2}$
−0.5	−5.9498	7.0276
−0.3	−6.5698	7.7449
0.0	−7.6626	9.0060
0.5	−9.9681	11.6585
1.0	−12.8856	15.0059

ARTICLE

5. CONCLUSION

The ethylene glycol-based hybrid nanoparticles in a thin-film flow by persuaded magnetic field in a porous stretching sheet are discussed numerically. The numerical analysis demonstrated the suction/injection has an essential impact on the boundary layer flow and heat transfer in the MHD thin-film hybrid nanofluid. Some of the interesting findings include;

(i) It is found that both profiles showed the opposite trends when upsurging the value of parameters M and ϕ_2.

(ii) Growth of the parameters S, λ and w leads to decay the speed of particles and cool down the viscous hybrid nanofluid.

(iii) Both physical quantities diminished because of the overshot of the parameters M and ϕ_2.

(iv) Local skin friction towards the increasing parameters of S, λ and w curtail and reverse pattern is found for Nusselt number of the viscous hybrid nanofluid.

Last but not least, to boost the quality of the paper as well as knowledge in fluid mechanics, future work can be designed the new mathematical modelling to explore the several effects in a thin-film such as entropy generation, viscous dissipation, thermal radiation and more general effects. Some strategies include the different geometry like channel, cylinder, cone and more general geometry can be extended from this work.

NOMENCLATURE

Pr Prandtl number
t Time (s)
k Thermal conductivity $(\mathrm{Wm^{-1}K^{-1}})$
$h(t)$ Uniform thickness of a thin-film
S Dimensionless unsteadiness parameter
(u, v) Velocity components (x, y)
T Temperature (K)
C_ρ Specific heat at constant pressure $(\mathrm{Jkg^{-1}K^{-1}})$
T_w Surface temperature of the fluid (K)
T_0 Initial temperature of the fluid (K)
T_{ref} Reference temperature of the fluid (K)
α, b Positive constants
f Velocity profile
U_w Stretched velocity
V_w Velocity of suction/injection
M Magnetic interaction parameter
C_f Local skin friction
Nu_x Nusselt number
q_w Heat transfer rate $(\mathrm{Wm^{-2}})$
Re Reynold number
w Dimensionless suction/injection parameter
σ Electrical conductivity $(\Omega\mathrm{m})^{-1}$
ξ Thin-film thickness
ϕ Volume fraction of nanoparticles
ψ Physical stream function
η Similarity variable
θ Dimensionless temperature
ν Kinematic viscosity $(\mathrm{m^2s^{-1}})$
ρ Density $(\mathrm{kgm^{-1}s^{-1}})$
μ Effective dynamic viscosity $(\mathrm{kgm^{-1}s^{-1}})$
λ Dimensionless thin-film thickness
τ_w Wall shear stress (Pa)

Conflict of Interest

The authors declare no conflicts of interest.

Acknowledgments: The authors would like to acknowledge the Ministry of Higher Education Malaysia) for financial support through vote numbers FRGS/1/2019/STG06/UTM/02/4.

References and Notes

1. A. Bertozzi, *Zeitschrift Fur Angewandte Mathematik Und Mechanik* 76, 373 **(1996)**.
2. R. Roy, A. Roberts, and M. Simpson, *Journal of Fluid* 454, 235 **(2002)**.
3. A. Dutta, S. Som, and P. Das, *Journal Heat Transfer* 126, 906 **(2004)**.
4. D. Taherzadeh, Mechanics and Substrate Transport of Moving Biofilm Structures. Technische Universität München **(2011)**.
5. Y. Liu, M. Itoh, and H. Kyotoh, *Fluid Dynamics Research* 49, 055501 **(2017)**.
6. M. J. Kreder, D. Daniel, A. Tetreault, Z. Cao, B. Lemaire, J. V. Timonen, and J. Aizenberg, *Physical Review X* 8, 031053 **(2018)**.
7. M. Girtan, Future Solar Energy Devices. Springer, Angers, France **(2018)**, pp. 45–75.
8. M. Girtan, *Solar Energy* 195, 446 **(2020)**.
9. U. Thiele, *Colloids and Surfaces A: Physicochemical and Engineering Aspects* 553, 487 **(2018)**.
10. K. Seshan, Handbook of Thin Film Deposition Processes and Techniques. William Andrew **(2001)**.
11. C. Wang, *Quarterly of Applied Mathematics* 48, 601 **(1990)**.
12. B. Sakiadis, *AIChE J.* 7, 221 **(1961)**.
13. L. J. Crane, *Zeitschrift für Angewandte Mathematik und Physik ZAMP* 21, 645 **(1970)**.
14. P. Carragher and L. Crane, *ZAMM-Journal of Applied Mathematics and Mechanics/Zeitschrift für Angewandte Mathematik und Mechanik* 62, 564 **(1982)**.
15. H. I. Andersson, J. B. Aarseth, and B. S. Dandapat, *Int. J. Heat Mass Transfer* 43, 69 **(2000)**.
16. C. Wang, *Heat Mass Transfer.* 42, 759 **(2006)**.
17. S. Choi, *American Society of Mechanical Engineers, Fluids Engineering Division (Publication)* FED 231, 99 **(1995)**.
18. S.-S. Bi, L. Shi, and L.-L. Zhang, *Appl. Therm. Eng.* 28, 1834 **(2008)**.
19. D. Wen and Y. Ding, *J. Nanopart. Res.* 7, 265 **(2005)**.
20. K. Das, N. Acharya, and P. K. Kundu, *Thermal Science* 21, 2369 **(2017)**.
21. W. A. Khan and I. Pop, *Int. J. Heat Mass Transfer* 53, 2477 **(2010)**.
22. Y. Yirga and B. Shankar, *International Journal for Computational Methods in Engineering Science and Mechanics* 16, 275 **(2015)**.
23. O. Pourmehran, M. Rahimi-Gorji, and D. D. Ganji, *Journal of the Taiwan Institute of Chemical Engineers* 65, 162 **(2016)**.
24. S. Jahan, H. Sakidin, R. Nazar, and I. Pop, *J. Mol. Liq.* 261, 550 **(2018)**.
25. M. E. Hafidz, Hafidzuddin, K. Naganthran, R. Nazar, and N. M. and Arifin, *Journal of Physics: Conference Series* 1366, 27 **(2019)**.
26. K. Gangadhar, T. Kannan, K. DasaradhaRamaiah, and G. Sakthivel, *International Journal of Ambient Energy* 41, 969 **(2020)**.

27. M. V. Krishna and A. J. Chamkha, *Journal of Porous Media* 22, 209 **(2019a)**.
28. M. V. Krishna and A. J. Chamkha, *Results in Physics* 15, 26 **(2019b)**.
29. A. J. Chamkha, M. A. Mansour, A. M. Rashad, H. Kargarsharifabad, and T. Armaghani, *J. Thermophys Heat Transfer* 34, 836 **(2020)**.
30. S. Hazarika, S. Ahmed, and A. J. Chamkha, *Mathematics and Computers in Simulation* 182, 819 **(2021)**.
31. A. J. Chamkha, A. S. Dogonchi, and D. D. Ganji, *Applied Sciences* 8, 2396 **(2018)**.
32. A. S. Dogonchi, S. M. Seyyedi, M. Hashemi-Tilehnoee, A. J. Chamkha, and D. D. Ganji, *Case Studies in Thermal Engineering* 30, 59 **(2019)**.
33. A. S. Dogonchi, M. Waqas, S. R. Afshar, S. M. Seyyedi, M. Hashemi-Tilehnoee, A. J. Chamkha, and D. D. Ganji, *International Journal of Numerical Methods for Heat & Fluid Flow* 30, 59 **(2020)**.
34. S. Devi and S. Devi, *International Journal of Nonlinear Sciences and Numerical Simulation* 17, 249 **(2016)**.
35. S. S. U. Devi and S. A. Devi, *Can. J. Phys.* 94, 490 **(2016)**.
36. S. U. Devi and S. A. Devi, *Journal of the Nigerian Mathematical Society* 36, 419 **(2017)**.
37. S. Suresh, K. Venkitaraj, P. Selvakumar, and M. Chandrasekar, *Colloids and Surfaces A: Physicochemical and Engineering Aspects* 388, 41 **(2011)**.
38. I. Waini, A. Ishak, and I. Pop, *Int. J. Heat Mass Transfer* 136, 288 **(2019)**.
39. I. Waini, A. Ishak, and I. Pop, *Phys. Scr.* 94, 2 **(2019)**.
40. I. Waini, A. Ishak, and I. Pop, *International Journal of Numerical Methods for Heat & Fluid Flow* 29, 3110 **(2019)**.
41. M. Ghalambaz, A. Doostani, E. Izadpanahi, and A. J. Chamkha, *J. Therm. Anal. Calorim.* 139, 2321 **(2020)**.
42. T. Tayebi and A. J. Chamkha, *Journal of Thermal Science and Engineering Applications* 12, 031009 **(2019)**.
43. M. VeeraKrishna, G. Subba Reddy, and A. Chamkha, *Physics of Fluids* 30, 023106 **(2018)**.
44. M. VeeraKrishna and A. J. Chamkha, *Physics of Fluids* 30, 053101 **(2018)**.
45. M. V. Krishna, K. Jyothi, and A. J. Chamkha, *Journal of Porous Media* 23, 751 **(2020)**.
46. M. V. Krishna, P. Anand, and A. J. Chamkha, *Special Topics & Reviews in Porous Media: An International Journal* 10, 203 **(2019)**.
47. M. V. Krishna, M. G. Reddy, and A. J. Chamkha, *International Journal of Fluid Mechanics Research* 46, 1 **(2019)**.
48. M. Veera Krishna, N. Ameer Ahamad, and A. J. and Chamkha, *Alexandria Engineering Journal* 60, 845 **(2021)**.
49. T. Cebeci and P. Bradshaw, Physical and Computational Aspects of Convective Heat Transfer. New York, Springer **(1988)**.
50. N. A. Rawi, M. R. Ilias, Y. J. Lim, Z. M. Isa, and S. Shafie, *Journal of Physics: Conference Series* 890, 012048 **(2017)**.
51. K. Ahmad, Z. Wahid, and Z. Hanouf, *Journal of Physics: Conference Series* 1127, 20 **(2019)**.
52. R. K. Tiwari and M. K. Das, *Int. J. Heat Mass Transfer* 50, 2002 **(2007)**.
53. N. Sandeep, R. P. Sharma, and M. Ferdows, *J. Mol. Liq.* 234, 437 **(2017)**.
54. N. Sandeep, *Adv. Powder Technol.* 28, 865 **(2017)**.
55. H. Upreti, A. K. Pandey, and M. Kumar, *Alexandria Engineering Journal* 57, 1839 **(2018)**.
56. D. Pal, *Computers & Mathematics with Applications* 66, 1161 **(2013)**.
57. S. Das, S. Guchhait, R. Jana, and O. Makinde, *Alexandria Engineering Journal* 55, 1321 **(2016)**.